

Nanoscale

Accepted Manuscript



This is an *Accepted Manuscript*, which has been through the Royal Society of Chemistry peer review process and has been accepted for publication.

Accepted Manuscripts are published online shortly after acceptance, before technical editing, formatting and proof reading. Using this free service, authors can make their results available to the community, in citable form, before we publish the edited article. We will replace this *Accepted Manuscript* with the edited and formatted *Advance Article* as soon as it is available.

You can find more information about *Accepted Manuscripts* in the [Information for Authors](#).

Please note that technical editing may introduce minor changes to the text and/or graphics, which may alter content. The journal's standard [Terms & Conditions](#) and the [Ethical guidelines](#) still apply. In no event shall the Royal Society of Chemistry be held responsible for any errors or omissions in this *Accepted Manuscript* or any consequences arising from the use of any information it contains.



Journal Name

ARTICLE

Received 00th January 20xx,
Accepted 00th January 20xx
DOI: 10.1039/x0xx00000x

www.rsc.org/

Post passivation light trapping back contacts for silicon heterojunction solar cells

M. Smeets,^a K. Bittkau,^a F. Lentz,^a A. Richter,^a K. Ding,^a R. Carius,^a U. Rau^a and U. W. Paetzold^{a,b,c}

Light trapping in crystalline silicon (c-Si) solar cells is an essential building block for high efficiency solar cells targeting low material consumption and low costs. In this study, we present the successful implementation of highly efficient light-trapping back contacts, subsequent to the passivation of Si heterojunction solar cells. The back contacts are realized by texturing an amorphous silicon layer with a refractive index close to the one of crystalline silicon at the back side of the silicon wafer. As a result, decoupling of optically active and electrically active layers is introduced.

In the long run, the presented concept has the potential to improve light trapping in monolithic Si multijunction solar cells as well as solar cell configurations where texturing of the Si absorber surfaces usually results in a deterioration of the electrical properties. As part of this study, different light-trapping textures were applied to prototype silicon heterojunction solar cells. The best path length enhancement factors, at high passivation quality, were obtained with light-trapping textures based on randomly distributed craters. Comparing a planar reference solar cell with an absorber thickness of 280 μm and additional anti-reflection coating, the short-circuit current density (J_{sc}) improves for a similar solar cell with light-trapping back contact. Due to the light trapping back contact, the J_{sc} is enhanced around 1.8 mA/cm^2 to 38.5 mA/cm^2 due to light trapping in the wavelength range between 1000 nm and 1150 nm.

Introduction:

Today, a significant part of research in the field of photovoltaics aims at reducing the costs of crystalline silicon solar cells. The most popular approaches are (i) applying thinner mono-crystalline absorber layers as well as (ii) applying cheaper poly-crystalline absorber layers, while maintaining high power conversion efficiencies^{1–4}. Both approaches are driven by the fact that around 23 % of the solar module costs are still caused by producing the Si wafer itself⁵.

Light trapping is an essential component of maintaining high power conversion efficiencies in crystalline silicon solar cells, as it compensates to large amount for the low absorptance of crystalline silicon close to the band gap energy^{6,7}. In commercial monocrystalline silicon solar cells, wet chemically etched randomly distributed pyramids in the dimensions ranging from 3 μm to 8 μm act as light-trapping textures. But, the material consumption of the Si wafer during this wet chemical etching process is quite significant^{8,9}. This loss has only been tolerated so far, as the pyramids induce highly efficient light incoupling as well as light trapping, which usually

results in an enhanced power conversion efficiency^{10,11}.

When aiming at Si wafer thicknesses below 20 μm and a maximum of material usage, light management with randomly distributed pyramids causes several severe limitations for the advancement of silicon solar cells: i) The dimension of the pyramids as well as the associated material losses are no more compatible with very thin Si wafers, e.g. thicknesses smaller than 20 μm . ii) The open-circuit voltage (V_{oc}) of the textured c-Si solar cells is easily lowered compared with planar c-Si solar cells, since the quality of the passivation can suffer when deposited on textured surfaces iii) Texturing the front side of Si wafers is challenging for several solar cell concepts as discussed in the following. E.g. for solar cells based on liquid phase crystallized silicon^{12,13}, texturing the front side is not a straight forward process, as the material properties of the c-Si absorber, with thicknesses of 20 μm or less, can easily degrade during crystallization on textured surfaces¹⁴. Also for monolithic multijunction concepts with c-Si bottom solar cell, e.g. perovskite-c-Si tandem solar cells planar c-Si solar cells are essential. Till today, perovskite layers have not successfully been processed from solution on top of randomly distributed

^a Forschungszentrum Jülich GmbH IEK-5 Photovoltaics, Germany

^b IMEC – Partner in Solliance, Kappeldreef 75, Leuven, B-3001

^c Karlsruhe Institute of Technology, Institute of Microstructure Technology, 76344 Eggenstein-Leopoldshafen, Germany

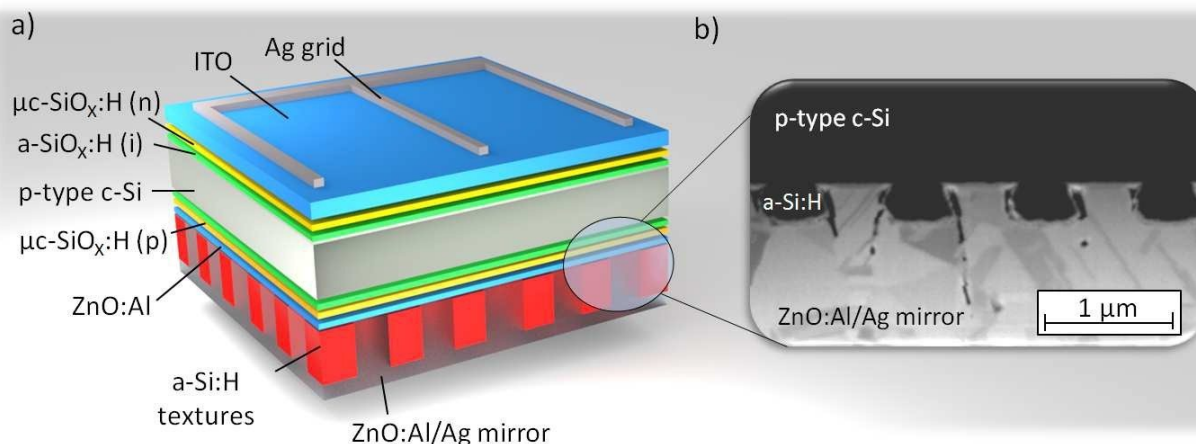


Figure 1: Sketch of a) a planar silicon heterojunction (SHJ) solar cell, applying a post passivation light trapping back contact (PPLTBC) based on a binary grating b) Cross-section of a SHJ solar cell applying the PPLTBC concept based on a binary grating texture imaged by SEM.

pyramids. Applying novel nanophotonic light-trapping textures to c-Si solar cells is a promising route to tackle these challenges, i.e. offering low material losses and small variations of the surface height. The nanoscale textures can be compatible even with Si wafers of thicknesses in the dimension of a few μm ^{15–19} and to perovskite solar cells processed on top by spin coating²⁰.

For thin Si solar cells in the μm range, excellent light management using Si wafers with nanophotonic textures at the front contact has already been demonstrated by Trompoukis et al.^{18,21}. However, passivating the nanophotonic Si surfaces appeared to be challenging. A resulting passivation degradation as well as wafer damaging easily results in increased surface recombination and thus lower V_{oc} . To prevent degradation, light-management textures shall be processed subsequent to planar passivation layers. Based on this approach, improved absorptance compared to planar reference solar cells due to light trapping with binary shaped nanophotonic grating back contacts were reported^{19,22,23}. In 2015 and 2016, Tucher et al.²⁴ and Eisenlohr et al.²⁵ published on PERT solar cells with an efficiency gain due to the application of binary grating back contacts. Further improvements in light-trapping efficiency could be achieved by varied 3D geometries, either randomly distributed or designed for special light-trapping properties, as known from the so-called super cell designed by the group of Thomas Krauss for efficient light-management at the front side²⁶.

As literature shows, efficient light trapping in Si solar cells with nanophotonic textures can be achieved at the front side as well as the back side. In this work we implement different 3D light-trapping textures at the back side of SHJ solar cells. In order to implement 3D textures like binary gratings and textures beyond in SHJ solar cells, we present a reactive ion etching process chain to fabricate nanophotonic post passivation light trapping back contacts (PPLTBC). Therefore, the textures replicated by nanoimprint lithography are transferred from the nanopatterned photoresist layer to a

hydrogenated amorphous silicon (a-Si:H) layer, deposited subsequent to all passivation layers. We demonstrate a precise transfer of different textures, including binary gratings as well as randomly distributed crater-like textures, on the micrometer scale and the nanometer scale. Similar process parameters were applied to transfer both surface textures. Furthermore, the resulting textures are implemented in silicon heterojunction solar cells acting as PPLTBC. We investigate the light-trapping properties of the applied nanophotonic textures and show improved light trapping with the implemented texture based on randomly distributed craters compared to a binary grating²³. Simultaneously, the fill factor as well as the V_{oc} is maintained, due to the planar high quality passivation layers. Combining the PPLTBC with a front side anti-reflection coating consisting of ITO covered with MgF_2 , the highest short-circuit current density (J_{sc}) achieved is 38.5 mA/cm^2 . This is an enhancement of around 2.3 mA/cm^2 compared with a planar reference solar cell applying only ITO at the front side. It will be shown that the gain is caused by a combination of improved anti-reflection and light-trapping effect. The latter accounts for 1.8 mA/cm^2 .

Materials and methods:

This study was conducted on SHJ solar cells with an absorber thickness of around $280 \mu\text{m}$ and a solar cell area of 0.36 mm^2 . All solar cells were processed on the same passivated Si wafer (series resistance between 1Ω and 5Ω) with a minority charge carrier lifetime of around $362 \mu\text{s}$. The processes were carried out simultaneously to ensure optimal comparability. In Fig. 1a, the structure of a planar passivated SHJ solar cell with PPLTBC is shown. The processed SHJ solar cells consist of a p-type c-Si wafer equipped with passivation layers (a-SiO_x:H), field generating layers ($\mu\text{c-SiO}_x\text{:H}$) and indium tin oxide (ITO) on the front side as well as aluminium doped zinc oxide (ZnO:Al) the back side. More details on the various functional layers, deposition methods as well as the employed characterization techniques are reported elsewhere²⁷. Corresponding layer thicknesses are provided in the supplementary material. It

shall be noted that the investigated SHJ solar cells solely vary in the back contact processing. While the planar solar cell employs a planar ZnO:Al/Ag mirror, the devices with the PPLTBC are composed of textured a-Si:H layer sandwiched between the back side ZnO:Al and an additional ZnO:Al/Ag mirror. The implemented texture drafted in Fig. 1 is a binary grating. It shall also be noted that the textured a-Si:H layer is partially etched through at the bottom of the grating, providing an electrical contact between the ZnO:Al/Ag mirror and the ZnO:Al interlayer. This architecture results in a sufficiently low series resistance (4.6 Ω - 9.2 Ω for completed solar cells). The cross-section of such a processed SHJ solar cell with a binary grating based PPLTBC, imaged by scanning electron microscopy (SEM), is shown in Fig. 1b. The cross-section was prepared by focused ion beam (FIB) milling. The free standing nanophotonic grating at the back side can be identified.

Processing PPLTBCs:

In this section, the process chain to fabricate PPLTBCs is shown. The reactive ion etching (RIE) process was strongly modified compared to other studies, focusing on RIE etching of Si for solar applications^{19,28,29}. The strong modification of our process relates to an alternation of two different processes enabling the remarkable feature of manufacturing various textures with similar process parameters. Here, a maintaining texture geometry compared to the initially imprinted texture geometry is demonstrated for various textures. In general, we start from a Si-wafer with the passivation layers, field generating layers and TCOs prepared. Next, an a-Si:H layer is deposited at the back side TCO, here by plasma enhanced chemical vapour deposition (PECVD). The layer thickness is targeted according to the required height of the light-trapping textures, here 700 nm. The modified concept of texturing this layer is divided into the following steps (see Fig. 2):

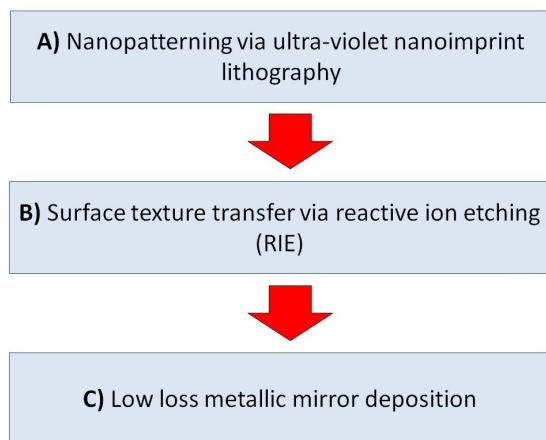


Figure 2: Flow diagram of the process chain to realize post passivation light trapping back contacts.

A) Ultra-violet nanoimprint lithography (UV NIL) is applied to replicate the light-trapping texture of the PPLTBC. UV NIL allows replicating various nearly arbitrary surface textures. Additionally, it is compatible with industrial up scaling via roll-to-plate imprint systems³⁰⁻³². In this work, diluted photoresist („Ormocomp“ provided by „micro resist technology GmbH) is spin coated at 3000 rpm for 30 s onto the amorphous silicon layer. In the next step, a polymer mold is used to transfer nanophotonic textures into the photoresist. Due to UV irradiation, the photoresist is cured. After removing the polymer mold, the light-trapping textures remain in the photoresist layer. More details on UV NIL can be found elsewhere^{30,32}. It should be mentioned that, generally, surface textures from binary gratings up to randomly distributed 3D textures can be replicated on highest quality.

B) After the UV NIL process, we use RIE etching steps to remove first the isolating residual resist and subsequently transfer the textures into a-Si:H with a RIE process applying alternating process parameters and gas mixtures. The applied RIE processes are established employing an „Oxford PlasmaLab 100“ with a chamber volume of 15.3 liters. I.e., for „process no. 1“ a gas mixture of CHF₃ and Ar is applied, using gas flows of 30 sccm and 10 sccm, respectively. To ignite stable plasmas, the forward power is set to 150 W, while the pressure is controlled to be 0.025 mbar. Applying these process parameters, the residual layer is removed after around 270 seconds.

As a result, the a-Si:H is partly uncovered. „Process no. 1“ was applied to form nanophotonic light trapping back contacts based on a low refractive index material in one of our previous study²³. Applying „process no. 1“ to transfer the textures from the photoresist to the amorphous silicon would morph the surface texture, as the etch rates of the materials differ significantly. For this reason, we developed a RIE routine, which alternates repeatedly between two etch processes, as known from the famous „Bosch process“³³.

(i) After the residual layer removal „process no. 2“ applying a gas mixture of SF₆ and Ar, with gas flows of 10 sccm and 30 sccm, respectively, is applied for 15 s. The forward bias is set to 100 W for a pressure of 0.02 mbar.

(ii) Next, „process no. 1“ is again applied for 15 s as well. Multiple repeated alternations (~15 for this thickness) of these two processes results in a high quality texture transfer from the photoresist to the a-Si:H layer in around 9 min.

This high quality transfer of various textures to a-Si:H is innovative for the field of photovoltaics as it allows accessing a much broader range of light trapping textures than possible before. The broad range of textures is accessible, as each applied process etches the respective material selectively.

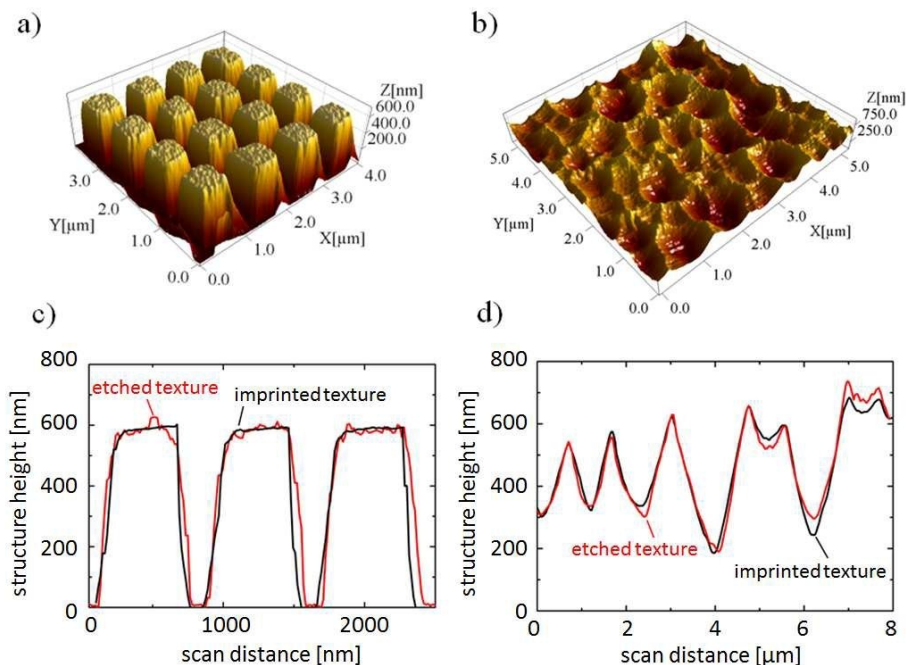


Figure 3: 3D plots of an AFM surface scan, again, of a nanophotonic grating (a) and randomly distributed textured transferred from photoresist to amorphous silicon. Line scans of the imprinted and transferred textures at the same position for both types of textures are shown in c) and d).

Due to the very short alternation times, the imprinted 3D geometry of the light-trapping textures is maintained, as underetching of the photoresist layer is prevented. In Fig. 3, AFM surface scans as well as AFM line scans of the imprinted textures and the textures etched into the amorphous silicon are presented. Here, AFM line scans of a binary grating as well as randomly distributed craters are compared after the imprint and in the transferred state after dry etching. The AFM line scans demonstrate the well reproduced texture heights and surface angles.

C) In a last step, a back reflector consisting of 50 nm ZnO:Al and 500 nm Ag is deposited. The ZnO:Al layer is essential in order to reduce parasitic losses at the Ag surface caused by plasmonic effects. Embedding the metal surface in materials with a refractive index of $n < 2$, results in a shift of the excitation wavelength of these plasmonic losses from the relevant wavelengths range to shorter wavelengths^{34–36}.

Results:

Solar cells with planar passivation and PPLTBC:

In order to demonstrate the technological advantages of PPLTBC for light trapping induced at the back side of Si solar cells, prototype SHJ solar cells with the layer stacks according to Fig. 1 and different back contacts, were processed. The

different types of PPLTBCs were: (i) planar back contacts, serving as reference solar cells, (ii) PPLTBC based on a binary grating with a period of 1000 nm. This grating period was chosen based on publication working on the optimization of grating back contacts^{22,37}. The width and heights are around 500 nm and 600 nm, respectively. (iii) PPLTBC based on randomly distributed craters, which have shown excellent light trapping capabilities for thin-film silicon solar cells³⁸. An overview of the solar cell parameters of the champion solar cells during this study is given in table 1. The corresponding IV-curves are provided in the supplementary material. It can be seen that the fill factor (FF) of a solar cell applying the grating based PPLTBC shows a similar value around 75 % compared with the planar reference solar cells. A small decrease for case (iii) to a FF around 73 % can be well explained with an increased series resistance, likely due to a not optimal contact. It shall be noted that the external quantum efficiency measurements are independent on external bias voltage, indicating a similar charge carrier collection efficiency for all solar cells.

Analyzing the open-circuit voltage (V_{OC}) provides information about the passivation quality. Similar values of around 645 mV for all processed prototype SHJ solar cells were measured. Thus, degradation of the planar passivation layers due to the applied process chain can be neglected.

Table 1: Overview of the solar cell parameters for a planar reference SHJ solar cell as well as SHJ solar cells applying PPLTBC textures processed during the same depositions. Solar cells with single anti-reflection coating (SARC) and double anti-reflection coating (DARC) are listed.

	Planar (SARC)	Planar (DARC)	Binary grating (SARC)	Ran. distributed craters (SARC)	Ran. distributed craters (DARC)
FF [%]	74.9	74.9	75.1	72.9	72.9
V_{OC} [mV]	646	646	645	646	646
J_{SC} [mA/cm ²]	36.2	36.6	37.0	37.4	38.5
PCE [%]	17.5	17.71	17.91	17.6	18.15
R_S [Ω]	4.8	4.8	4.6	9.2	9.2
R_{SH} [k Ω]	7.6	7.6	3.3	4.8	4.8

The most significant parameter, by means of light trapping, is the short-circuit current density (J_{SC}) of the SHJ solar cells. The lowest J_{SC} , namely 36.20 mA/cm², was measured for the planar reference SHJ solar cell with single anti-reflection coating (SARC). Implementing the binary grating based PPLTBC as well as the PPLTBC based on randomly distributed craters increases this value to around 36.98 mA/cm² and 37.40 mA/cm², respectively.

Comparing the power conversion efficiencies (PCE) of the SHJ solar cells, the planar SHJ solar cell (with SARC) shows the lowest value. The PPLTBC, based on the randomly distributed

craters, leads to an increase of the PCE while the best PCE was reached with the binary grating based PPLTBC. The main reason for this result is the reduced FF of the SHJ solar cell applying the PPLTBC based on randomly distributed craters.

In order to spectrally resolve the light-trapping effect, the external quantum efficiencies of the SHJ solar cells as a function of the wavelengths of the incident light are shown in Fig. 4. As we aim at introducing light trapping to the solar cells, we focus on the EQEs of light of wavelengths > 900 nm, where the absorptance of Si wafers starts to decrease significantly.

For light of wavelengths between 900 nm and 1000 nm, the

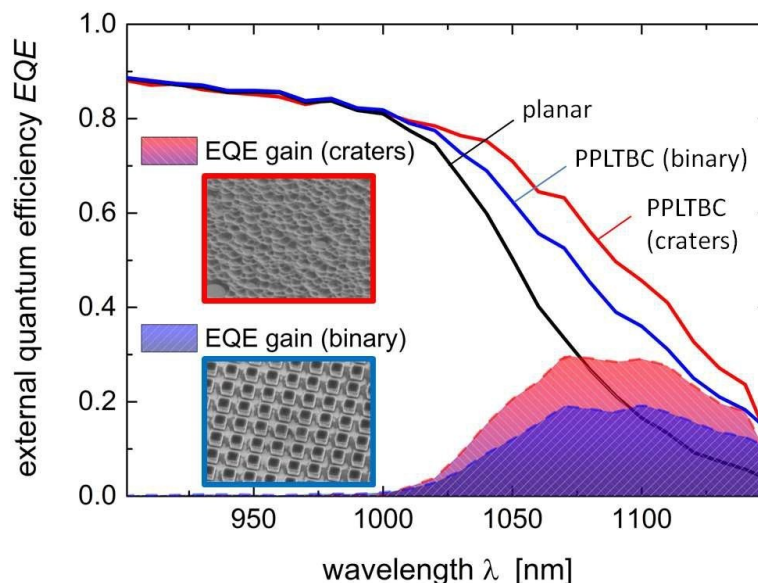


Figure 4: EQE of SHJ solar cells for wavelengths longer than 900 nm. The shaded areas represent the gain in EQE with PPLTBC textures compared to a polished reference solar cell. SEM images are used to visualize the applied PPLTBC textures.

EQEs of the SHJ solar cells remain similar. Increased *EQEs* are found for the prototype solar cells applying PPLTBC for wavelengths longer than 1000 nm. In detail, the binary grating based PPLTBC already shows a strong increase, but the *EQE* is enhanced even further for the application of the PPLTBC based on the randomly distributed craters. This result is in accordance to the increased J_{SC} . From these results, we conclude that light trapping with our crater-like textures can be very efficient, and can outperform light trapping with our binary grating. From simulations, even stronger enhancement due to implementing pyramid-like textures, either randomly distributed or periodically arranged at the surface can be expected^{17,37}.

To highlight the light-trapping effect of both PPLTBC textures, the gain in *EQE* compared to the planar reference (*EQE* prototype – *EQE* planar) SHJ solar cell is plotted in Fig. 4, additionally. The integral areas are shaded in the same color as the *EQE* curves.

Interaction of PPLTBC and anti-reflection coatings:

Having identified a very good light-trapping texture, in the subsequent step, we improve the light incoupling by changing the SARC to a DARC. The latter consist of a MgF_2 layer with a thickness of around 85 nm deposited on the ITO front contact. As a result, reflection losses at the TCO-air interface of the processed prototype solar cells can be reduced. We are

comparing the following cases.

(i) Planar solar cells with ITO-SARC and double anti-reflection coating (DARC) consisting of ITO and MgF_2 : An increase of the J_{SC} of 0.4 mA/cm² to 36.6 mA/cm² is measured when applying the additional MgF_2 layer is realized. The additionally generated J_{SC} is a result of improved light incoupling at the front side of the Si wafer.

(ii) The gain in J_{SC} when applying a PPLTBC (craters) compared to a planar solar cell:

For the solar cells with SARC, the highest enhancement of the J_{SC} induced by the PPLTBC was around 1.2 mA/cm².

For solar cells applying DARC and the same PPLTBC an enhancement of 1.8 mA/cm² is realized. All solar cell parameters are documented in table 1.

To investigate the origin of the enhanced J_{SC} , the *EQEs* of the planar SHJ solar cell (DARC) and the SHJ solar cell applying the PPLTBC based on the randomly distributed craters (DARC) are shown in Fig. 5, for wavelengths between 900 nm and 1150 nm. A remarkably increased *EQE* is measured for light of all wavelengths longer than 1000 nm for the solar cell with PPLTBC. It can be seen that the PPLTBC based on the randomly distributed craters significantly outperforms the planar reference solar cell due to the excellent light-trapping properties. Compared to the planar reference solar cell, the

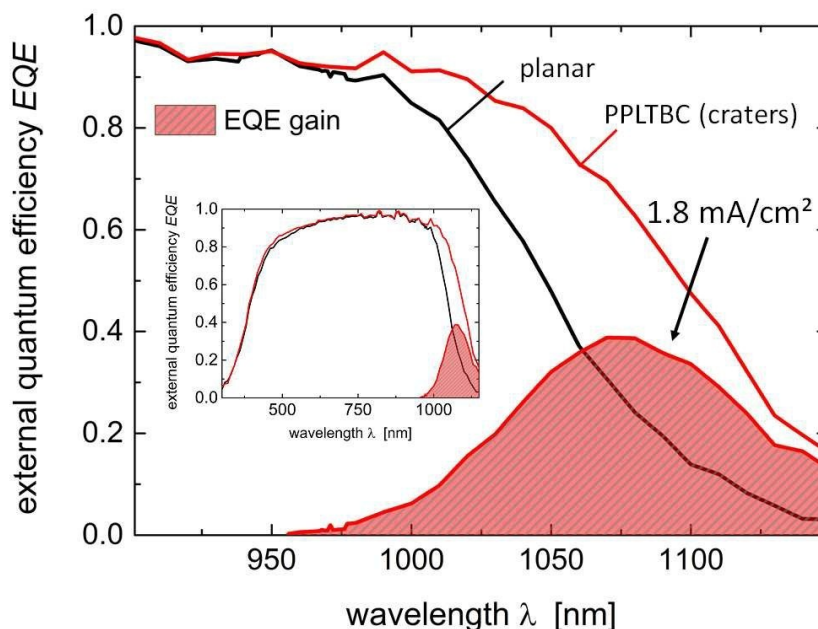


Figure 5: *EQEs* of SHJ solar cells for wavelengths longer 900 nm. The light trapping for a device with a PPLTBC based on randomly distributed textures and a planar back contact is compared for SHJ solar cells apply a double anti-reflection coating. The *EQE* gain compared to the polished reference solar cell is represented by the shaded area. The inset shows the *EQEs* for a wavelengths range between 300 nm and 1150 nm.

highest gain in *EQE* is around 0.40 for a wavelength of 1060 nm. The plus in *EQE* (shaded area) equals a J_{SC} of around 1.8 mA/cm². This result is of significance as we see a further increase of the light management due to the PPLTBC when applying an additional anti-reflection coating at the front interface (1.2 mA for SARC). The *EQEs* of the prototype solar cells for the full wavelength range can be seen in the inset of Fig. 5. Both *EQEs* are similar for light of the wavelength range between 300 nm and 1000 nm. The J_{SC} for both solar cells are 36.6 mA/cm² (planar) and 38.5 mA/cm² (PPLTBC). The resulting *PCEs* are 17.7 % and 18.15 %, respectively.

(iii) Planar solar cell with SARC compared to a solar cell with PPLTBC (craters) and DARC. It should be highlighted that due to the combination of DARC and PPLTBC improved light incoupling and light trapping are introduced, respectively. The overall gain in J_{SC} is around 2.3 mA/cm². This increase even compensates the slightly reduced FF and results in an absolute increase of η of around 0.7 %.

Path length enhancement factor:

To place our results in the context of literature, the path length enhancement factor (w) of our best solar cell will be compared to w of established concepts, in Fig 6. To determine w , we apply the established equation³⁹:

$$w(\lambda) = \frac{-\ln(1 - EQE(\lambda))}{\alpha_{c-Si} \cdot d_{c-Si}}$$

Here, α_{c-Si} is the absorption coefficient of crystalline silicon and d_{c-Si} is the thickness of the absorber layer. In Fig. 6, different values of w are compared for (i) a planar reference SHJ solar cell (black line), (ii) a SHJ solar cell with PPLTBC based on randomly distributed craters (red line), (iii) a SHJ solar cell with

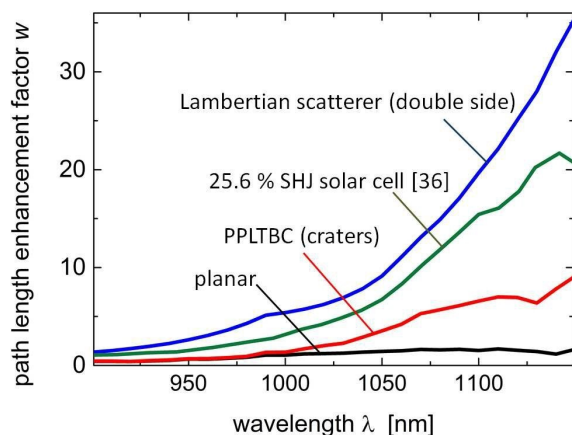


Figure 6: Path length enhancement factor of various light trapping concepts for wafer based silicon solar cells.

a power conversion efficiency of 25.6 % published in 2014⁴⁰ (green line) and (iv) a solar cell applying a Lambertian scatterer for a c-Si wafer thickness of 280 μm (blue line).

As the planar back contact reflects the incident light with negligible scattering, w increases only slightly towards longer wavelengths. In detail, w reaches a value of 1 around 1000 nm and increases up to 1.67 for 1150 nm. For all other SHJ solar cells, where scattering of light at the front or back side of the Si-wafer occurs, w increases with a larger slope towards longer wavelengths. For the best SHJ solar cell during this study (PPLTBC based on randomly distributed craters), w reaches a value slightly higher than 1 at 1000 nm. Towards longer wavelengths, this value increases with a significantly larger slope than seen for the planar solar cell and is enhanced for all wavelengths. The maximum of 9.3 is reached at 1150 nm solely due to scattering of light at the back contact. Comparing w to the values reached in solar cells applying a Lambertian scatterer or randomly distributed pyramids, w shows further improvement. For randomly distributed pyramids, w reaches a value of 20.6 for light of the wavelengths of 1150 nm. For a Lambertian scatterer (double side) a value of 35 is reached.

The advantage of both the latter concepts is an excellent anti-reflection effect combined with scattering of light already at the textured front side. Thus, a combination of PPLTBCs with textured front sides seem to be an interesting field to be investigated in future studies. Overall, the results of solar cells applying PPLTBCs are very promising.

Thus, implementing PPLTBCs applying the presented process shows the potential to additionally improve conventional light-management concepts due to the possibility to access novel light-trapping textures optimized by simulations^{17,37} without passivation degradation. Especially, for solar cell concepts where implementing light trapping by texturing the front side is not straight forward, applying PPLTBCs can come up as one very promising light-trapping concepts. One example could be solar cells based on liquid phase crystallized silicon where texturing the front interface can easily result in increased recombination centers inside the absorber.

Conclusion:

In this work, we report on the fabrication and implementation of amorphous silicon based light trapping back contacts prepared subsequent to the passivation of SHJ solar cells. This concept enables a decoupling of the optically active and electrically active layers of silicon heterojunction solar cells.

Efficient light trapping is demonstrated by implementing amorphous silicon based binary and crater-like textures at the back side of SHJ solar cells. Accessing nearly arbitrary light-trapping textures is realized by the combination of UV nanoimprint lithography and an optimized reactive ion etching

routine, developed throughout this work.

We demonstrate similar open-circuit voltages and fill factors as compared to planar solar cells when applying these back contacts to silicon heterojunction solar cells with a thickness of around 280 μm . The highest measured short-circuit current density was 38.5 mA/cm^2 realized by the implementation of back contacts based on randomly distributed craters interacting with a double anti-reflection coating consisting of ITO and MgF_2 at the front side. Compared to a planar solar cell of the same thickness, this is a gain of 1.8 mA/cm^2 . The corresponding path length enhancement factor increases up to a wavelength of 1150 nm to around 10. We regard this implementation process chain to be perfectly applicable to liquid phase crystallized silicon based solar cells or monolithic perovskite c-Si tandem solar cells.

Acknowledgement:

The authors gratefully acknowledge Andre Hoffmann, Thomas Kirchartz and Malte Köhler for fruitful discussions. Moreover, we would like to thank Hildegard Siekmann, Peter Hennig, Manuela Meyer and the colleagues of the "Helmholtz nanoelectronic facility" for technical support. The scientific work was partly funded by the European Commission through the 7th Framework Program grant no. 609788 (CHEETAH). The work of Ulrich Wilhelm Paetzold was funded by the German Academic Exchange Service.

References:

- 1 D. Fujishima, H. Inoue, Y. Tsunomura, T. Asaumi and S. Taira, *IEEE Journal of Photovoltaics*, 2010, 3137–3140.
- 2 M. Moreno and P. R. I. Cabarrocas, *EPJ Photovoltaics*, 2010, **1**, 10301.
- 3 M. L. Brongersma, Y. Cui and S. Fan, *Nature materials*, 2014, **13**, 451–60.
- 4 S. De Wolf, A. Descoedres, Z. C. Holman and C. Ballif, *Green*, 2012, **2**, 7–24.
- 5 *International Technology Roadmap for Photovoltaic (ITRPV) 2015*, 2016.
- 6 M. A. Green and M. J. Keevers, *Progress in Photovoltaics: Research and Applications*, 1995, **3**, 189–192.
- 7 K. R. Catchpole and A. Polman, *Optics express*, 2008, **16**, 21793–800.
- 8 H. Seidel, S. Csepregi, A. Heuberger and H. Baumgärtel, *J. electrochem. Soc.*, 1990, **137**, 3612–3626.
- 9 O. Tabata, R. Asahl, H. Funabashi, K. Shimaoka and S. Sugfuyama, *Sensors and Actuators A*, 1992, **34**, 51–57.
- 10 P. Campbell and M. A. Green, *Journal of Applied Physics*, 1987, **62**, 243.
- 11 P. Campbell and M. A. Green, *Solar Energy Materials and Solar Cells*, 2001, **65**, 369–375.
- 12 D. Amkreutz, J. Müller, M. Schmidt, T. Hänel and T. F. Schulze, *Progress in Photovoltaics: Research and Applications*, 2011, 937–945.
- 13 J. Haschke, D. Amkreutz, L. Korte, F. Ruske and B. Rech, *Solar Energy Materials and Solar Cells*, 2014, **128**, 190–197.
- 14 C. Becker, V. Preidel, D. Amkreutz, J. Haschke and B. Rech, *Solar Energy Materials and Solar Cells*, 2015, **135**, 2–7.
- 15 Y. Park, E. Drouard, O. El Daif, X. Letartre, A. Fave, A. Kaminski, M. Lemiti and C. Seassal, *Optics express*, 2009, **17**, 14312–14321.
- 16 S. E. Han and G. Chen, *Nano Letters*, 2010, **10**, 4692–4696.
- 17 K. X. Wang, Z. Yu, V. Liu, Y. Cui and S. Fan, *Nano letters*, 2012, 10–13.
- 18 C. Trompoukis, O. El Daif, V. Depauw, I. Gordon and J. Poortmans, *Applied Physics Letters*, 2012, **101**, 103901.
- 19 A. Mellor, H. Hauser, C. Wellens, J. Benick, M. Peters, A. Guttowski, I. Tobias, A. Marti, A. Luque and B. Bläsi, *Optics Express*, 2013, **21**, 1926–1933.
- 20 U. W. Paetzold, W. Qiu, F. Finger, J. Poortmans and D. Cheyns, *Applied Physics Letters*, 2015, **106**, 173101.
- 21 C. Trompoukis, O. El Daif, P. P. Sharma, H. S. Radhakrishnan, M. Debucquoy, V. Depauw, K. Van Nieuwenhuysen, I. Gordon, R. Mertens and J. Poortmans, *Progress in Photovoltaics: Research and Applications*, 2014.
- 22 M. Peters, M. Rüdiger, H. Hauser, M. Hermle and B. Bläsi, *Progress in Photovoltaics: Research and Applications*, 2012.
- 23 M. Smeets, F. Lentz, A. Richter, Y. Augarten, K. Bittkau, K. Ding, R. Carius, U. Rau and U. W. Paetzold, *Physica Status Solidi (a)*, 2016, **213**, 1949–1954.
- 24 N. Tucher, J. Eisenlohr, H. Hauser, J. Benick, M. Graf, C. Müller, M. Hermle, J. C. Goldschmidt and B. Bläsi, *Energy Procedia*, 2015, **77**, 253–262.
- 25 J. Eisenlohr, N. Tucher, H. Hauser, M. Graf, J. Benick, B. Bläsi, J. C. Goldschmidt and M. Hermle, *Solar Energy Materials and Solar Cells*, 2016, **155**, 288–293.
- 26 E. R. Martins, J. Li, Y. Liu, J. Zhou and T. F. Krauss, *Physical Review B*, 2012, **86**, 041404.
- 27 A. Richter, F. Lentz, M. Meier, F. Finger and K. Ding, *Physica Status Solidi (a)*, 2016, **213**, 1976–1982.
- 28 W. A. Nositschka, C. Beneking, O. Voigt and H. Kurz, *Solar Energy Materials and Solar Cells*, 2003, **76**, 155–166.
- 29 Z. Liu, Y. Wu, B. Harteneck and D. Olynick, *Nanotechnology*, 2013, **24**, 015305.
- 30 H. Schiff, *Journal of Vacuum Science & Technology B: Microelectronics and Nanometer Structures*, 2008, **26**, 458.
- 31 H. Hauser, B. Michl, S. Schwarzkopf, V. Kübler, C. Müller, M. Hermle and B. Bläsi, *IEEE Journal of Photovoltaics*, 2012, **2**, 114–122.
- 32 M. Meier, U. W. Paetzold, M. Prömpers, T. Merdzhanova, R. Carius and A. Gordijn, *Progress in Photovoltaics: Research and Applications*, 2014, **22**, 1226–1236.
- 33 Patent on Bosch Process, Robert Bosch GmbH, Nr. 5.501.893, 1996.
- 34 F.-J. Haug, T. Söderström, O. Cubero, V. Terrazoni-Daudrix and C. Ballif, *Journal of Applied Physics*, 2008, **104**, 064509.
- 35 U. W. Paetzold, E. Moulin, B. E. Pieters, R. Carius and U. Rau, *Optics Express*, 2011, **19 Suppl 6**, A1219–1230.
- 36 E. Moulin, U. W. Paetzold, K. Bittkau, J. Owen, J. Kirchhoff, A. Bauer and R. Carius, *Progress in Photovoltaics: Research and Applications*, 2013, 1236–1247.
- 37 A. Mellor, I. Tobias, A. Marti and A. Luque, *Solar Energy Materials and Solar Cells*, 2011, **95**, 3527–3535.
- 38 J. Müller, B. Rech, J. Springer and M. Vanecek, *Solar Energy*, 2004, **77**, 917–930.
- 39 M. Berginski, B. Rech, J. Hüpkes, H. Stiebig and M. Wuttig, *SPIE Proceedings*, 2006, **6197**, 61970Y.
- 40 K. Masuko, M. Shigematsu, T. Hashiguchi, D. Fujishima, M. Kai, N. Yoshimura, T. Yamaguchi, Y. Ichihashi, T. Mishima, N. Matsubara, T. Yamanishi, T. Takahama, M. Taguchi, E. Maruyama and S. Okamoto, *IEEE Journal of Photovoltaics*, 2014, **4**, 1433–1435.